

# Topological Weyl semimetals in $\text{Bi}_{1-x}\text{Sb}_x$ alloys

Yu-Hsin Su,<sup>1</sup> Wujun Shi,<sup>1,2</sup> Claudia Felser,<sup>1</sup> and Yan Sun<sup>1,\*</sup>

<sup>1</sup>Max Planck Institute for Chemical Physics of Solids, D-01187 Dresden, Germany

<sup>2</sup>School of Physical Science and Technology, ShanghaiTech University, Shanghai 200031, China

We have investigated the Weyl semimetal (WSM) phases in bismuth antimony ( $\text{Bi}_{1-x}\text{Sb}_x$ ) alloys by the combination of atomic composition and arrangement. Via first principles calculations, we have found two WSM states with the Sb concentration of  $x = 0.5$  and  $x = 0.83$  with specific inversion symmetry broken elemental arrangement. The Weyl points are close to the Fermi level in both of these two WSM states. Therefore, it has a good opportunity to obtain Weyl points in Bi-Sb alloy. The WSM phase provides a reasonable explanation for the current transport study of BiSb alloy with the violation of Ohm's law [Dongwoo Shin *et al.*, Nature Materials 16, 1096 (2017)]. This work shows that the topological phases in Bi-Sb alloys depend on both elemental composition and their specific arrangement.

## I. INTRODUCTION

Weyl semimetal (WSMs) is topological metallic state with valence bands and conduction bands linearly touching in three dimensional momentum space via the Weyl points<sup>1,2</sup>. These Weyl points are doubly degeneracy and behave as the monopoles of Berry curvature with positive and negative chiralities, resulting in non-zero topological charges. Similar to topological insulators (TIs), WSMs also have topological protected surface states. Owing to the non-zero Berry flux between one pair of Weyl points with opposite chirality, the surface states present as non-closed Fermi arc connecting this pair of Weyl points, which have been observed in several WSMs via Angle-resolved photoemission spectroscopy (ARPES) and Scanning tunneling microscope (STM)<sup>3-13</sup>. Beside Fermi arc surface states, WSMs also host exotic transport properties in the bulk, such as chiral anomaly effect<sup>14-17</sup>, large magnetoresistance (MR)<sup>14-16,18-21</sup>, strong spin and anomalous Hall effect<sup>22-26</sup>, gravitational anomaly effect<sup>27</sup>, even special catalyst effect<sup>28</sup>.

There are already several WSMs were predicted, and some of them were experimentally verified by the observation of Fermi arcs on the surface<sup>3-13</sup> and negative MR in the bulk transports<sup>14-17</sup>. So far, most of the study about inversion symmetry broken WSMs are focused on the space group without inversion center. Besides the intrinsic space group without inversion symmetry, alloy is another efficient way to break inversion symmetry. Owing to the alloy-able of lots of semimetals, it offers a good opportunity to achieve WSMs in a large number of materials. That motives us to look back of the well known topological semimetals and semiconductors based on alloy, in which a typical example is the  $\text{Z}_2$  TI  $\text{Bi}_{1-x}\text{Sb}_x$ <sup>29-31</sup>.

$\text{Bi}_{1-x}\text{Sb}_x$  is the first experimentally discovered 3D  $\text{Z}_2$  TI<sup>30</sup>. Due to the similar lattice parameters for Bi and Sb,  $\text{Bi}_{1-x}\text{Sb}_x$  alloy can be experimentally formed and the composition can be artificially adjusted. Through atom substitution of Bi by Sb, a non-smooth band inversion happens along with the topological phase transition at

a Sb concentration of  $\approx 0.04$ <sup>30</sup>. The non-trivial band order can exist in a large range of Sb concentration after the phase transition<sup>32</sup>. Since there is not a global band gap for some Sb concentrations, the  $\text{Bi}_{1-x}\text{Sb}_x$  presents as a topological semimetal with inverted band gap<sup>29</sup>. In previous studies, the theoretical studies for  $\text{Bi}_{1-x}\text{Sb}_x$  were mainly based on the virtual crystal approximation keeping inversion symmetry as that in Bi and Sb<sup>32,33</sup>. However, owing to the chemical difference of elements Bi and Sb, the alloy of them should break the inversion symmetry. In combination with the inverted band order and semimetallic feature, the inversion symmetry broken arrangement in the alloy provides large possibility to realize WSM.

Recently, the chiral anomaly induced negative MR and violation of Ohm's law were observed in the transport measurements for Bi-Sb alloy, showing the emergence of WSM phase<sup>34,35</sup>. However, there is still a lack of fully investigation of the influence of the atomic arrangements in Bi-Sb alloy on their topological properties. In our present work, a systematic study on topological nature about the effect of composition and atomic arrangement in Bi-Sb alloy have been proposed and provides a detailed classification depending on the sort of topological phase, based on the quantitative first-principles calculations.

## II. METHODS

The density functional theory (DFT)-based first-principles calculations were performed by projected augmented wave (PAW) method as implemented in the Vienna *Ab-initio* Simulation Package (VASP)<sup>36</sup>. The exchange-correlation energy was considered in the generalized gradient approximation (GGA), following the Perdew-Burke-Ernzerhof (PBE)<sup>37</sup> parametrization scheme. The van der Waals interactions were also taken into account due to the layered lattice structure. In order to analyze the topological properties, we have projected the Bloch wavefunctions into maximally localized Wannier functions (MLWFs)<sup>38</sup>. The tight-binding model Hamiltonian parameters are determined from

the MLWFs overlap matrix. The surface state was considered under an open boundary conditions with the half-infinite model using the iterative Green's function method<sup>39,40</sup>.

### III. RESULTS

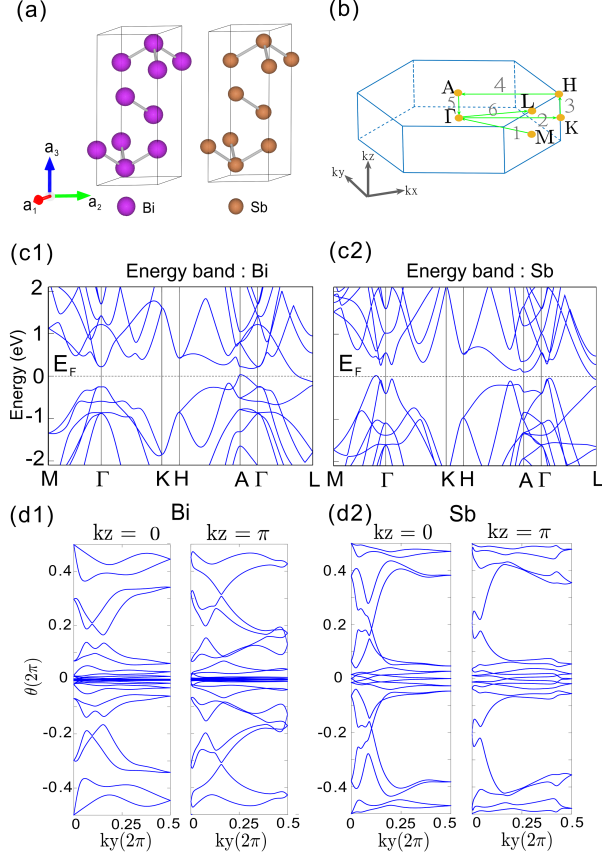


FIG. 1. (a) The hexagonal conventional unit cell of Bi and Sb atoms, consists of layered structure. The grey solid lines denote the intralayer bonding. (b) The Brillouin zone of hexagonal unit cell and the k-points path, containing high symmetry points, along which the band structure is calculated. (c) and (d) are the corresponding bulk energy band. (e, f) The evaluated Wannier centers on the plane  $k_z = 0$  and  $k_z = \pi$ , respectively.

Both Bi and Sb have the rhombohedral A7 crystal structure with space group  $R\bar{3}m$ , as indicated in Fig. 1(a). Consistent with previous reports, Bi and Sb have similar electronic band structures due to their similar chemical properties, see Fig. 1(c-d). Whereas, owing to different strength of spin-orbital coupling (SOC), they have different band orders and therefore different  $Z_2$  topological invariant of  $\nu_0 = 0$  and 1, respectively<sup>32,33</sup>, see Fig. 1(e-f). Based on the hexagonal lattice, we have investigated all atomic arrangements for different elements composition of  $x = 0.17, 0.33, 0.5, 0.67$ , and

0.83. In our calculations the band inversion between antisymmetric ( $L_a$ ) and symmetric ( $L_s$ ) orbitals happens at the concentration with  $x = 0.5$ , which agrees well with previous tight binding analysis. Above that the system presents as topological insulators or semimetals, in which the WSM states were found in one arrangement for the composition of  $x = 0.5$  and  $x = 0.83$ , respectively. For convenience, we will take the WSM phase in the compositions of  $x = 0.5$  as the example to introduce the electronic structure.

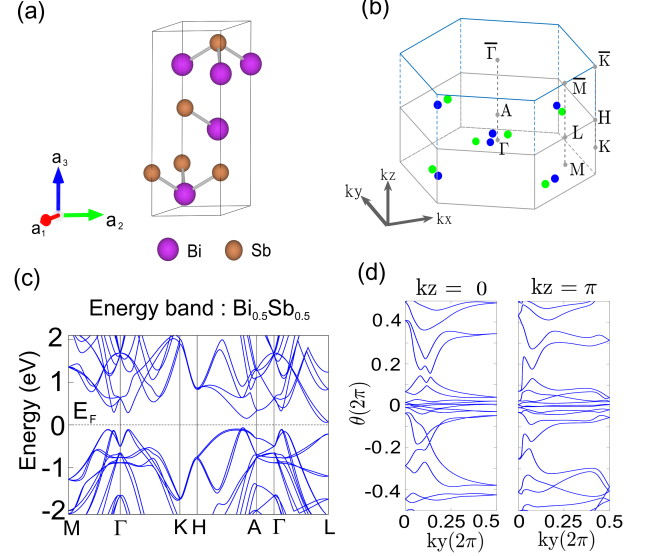


FIG. 2. (a) The fully relaxed crystal structure for  $\text{Bi}_{0.5}\text{Sb}_{0.5}$  with the specific arrangement of Bi and Sb atoms. (b) The 3D BZ of hexagonal unit cell where the location of Weyl points with positive chirality (blue) and negative chirality (green) are shown, and projected 2D BZ of (001) surface. (c) Bulk Energy band for specific  $\text{Bi}_{0.5}\text{Sb}_{0.5}$ . (d) The evaluated Wannier centers on the plane  $k_z = 0$  and  $k_z = \pi$ , respectively.

Fig. 2(a) shows the lattice structure of  $\text{Bi}_{0.5}\text{Sb}_{0.5}$  with the specific atomic arrangement, where Bi layer and Sb layer stacking with each other in c direction. Though the formation energy is slightly higher ( $\sim 3$  meV per formula unit) than that in the ground state arrangement, the energy difference is almost the limit of accuracy of the DFT itself. Therefore, it is reasonable to obtain this atomic arrangement in experiments. Owing to the absence of inversion symmetry, the spin degeneracy splits for all the bands, see Fig. 2(c), which also provides the possibility of Weyl points. The electronic band structure along high symmetry lines exhibits as a direct band gap insulator. To check the topological phase, we calculated the Wannier center evolutions in the high symmetry planes of  $k_z = 0$  and  $\pi$ , respectively. As shown in Fig. 2(d), the Wannier center curves calculated on the plane  $k_z = 0$  presents the existence of discontinuity, yet on plane  $k_z = \pi$  plane, the curves are always continuously connected. It indeed provides the evidence of a topological non-trivial phase in  $\text{Bi}_{0.5}\text{Sb}_{0.5}$ .

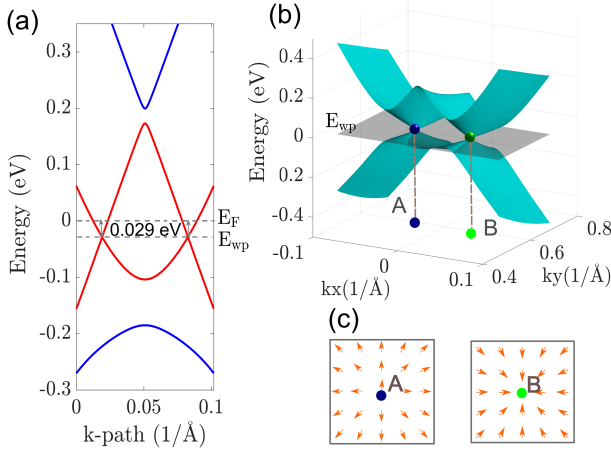


FIG. 3. (a) The energy band passing through two Weyl points, where  $E_F$  and  $E_{wp}$  represent the Fermi energy and the energy of Weyl points, respectively. The energy bands with color red denote the highest occupied band and the lowest unoccupied band. (b) The energy band structure around two Weyl points A and B on the plane  $k_z=0.4620(1/\text{\AA})$ . (c) The Berry curvature calculated on the two Weyl points A and B with normalization.

Though there is a general gap along high symmetry lines, its density of states (DOS) is not zero at Fermi level, implying a topological semimetal with bands cutting the Fermi level at some lower symmetry directions. Indeed, we found one pair of linear band crossings away from high symmetry points at  $(-0.031822, 0.592594, 0.245628)$  ( $1/\text{\AA}$ ) and  $(0.031808, 0.592380, 0.245608)$  ( $1/\text{\AA}$ ) as shown in Fig. 3. This pair of linear crossing points are Weyl cones behaving as the sink and source of Berry curvature. Considering the  $C_3$  rotation and time reversal symmetry, there are 6 pairs of Weyl points in total. Since the Weyl points is only around 30 meV bellow Fermi level, the Weyl points dominated phenomenons should be easy to detect by both surface technique and bulk transport measurements.

An important characteristic of WSM is the presence of surface Fermi arc states<sup>1</sup>. Considering the easy cleave-able bonding, we have chosen the (001) surface in our analysis. Fig. 4(a) and (b) illustrate the local DOS along two particular paths, one is passing through high symmetry lines of  $\bar{K}-\bar{\Gamma}-\bar{M}$ , and the other is across a pair of Weyl points with opposite chirality. Along the high symmetry lines of  $\bar{K}-\bar{\Gamma}-\bar{M}$  one can see that, besides the surface Dirac cone at  $\bar{\Gamma}$  points, there is the other surface bands on  $\bar{\Gamma}-\bar{M}$  line connecting bulk conduction and valence states. Since one pair of Weyl points with opposite chirality symmetrically locates on the two sides of  $\bar{\Gamma}-\bar{M}$  line, the additional surface bands should be the Fermi arc related states. To check this speculation, we directly plot surface energy dispersion along the k-path crossing one pair of Weyl points and perpendicular to  $\bar{\Gamma}-\bar{M}$ . As shown in Fig. 4(b), a surface bands merges into bulk via the Weyl points, just the typical feature

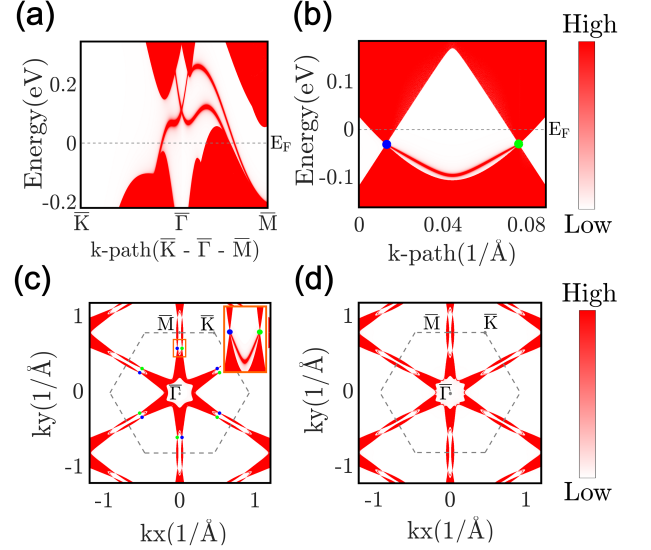


FIG. 4. (a) The local DOS of (001) plane calculated along a specific path passing through high symmetry points ( $\bar{K}-\bar{\Gamma}-\bar{M}$ ), where  $E_F$  denotes the Fermi energy. (b) The local DOS of (001) plane calculated along a path passing through two Weyl points. (c) The surface DOS on the (001) plane at the energy of Weyl points  $E_{wp}$ , where the Weyl points with positive (negative) chirality are denoted as blue (green) circles. and the grey dashed line represents the first BZ of the surface. The inset is the enlarged region around a pair of Weyl points. (d) The surface DOS on the plane (001) at the Fermi energy.

for the Fermi arc related states. Fixing the energy at Weyl points, one can easily found the Fermi arc starting from one Weyl points and end at the other see Fig. 4(c). Moreover, the Weyl points present as the linear touching of the projected bulk states. Hence, the  $\text{Bi}_{0.5}\text{Sb}_{0.5}$  is a type-II WSM. From the energy dispersions along  $\bar{\Gamma}-\bar{M}$  and one pair of Weyl points in Fig. 4(a-b), the Fermi arc related states can range in a large energy window from  $-0.1$  to  $0.2$  eV, hence the Fermi arcs can be also observed at Fermi level, see Fig. 4(e). Therefore, the WSMs in  $\text{Bi}_{0.5}\text{Sb}_{0.5}$  is further confirmed by the surface Fermi arcs.

Besides  $\text{Bi}_{0.5}\text{Sb}_{0.5}$ , the composition  $x = 0.87$  also shows WSMs state with Weyl points lying at  $(-0.00436, 0.721258, 0.275386)$  ( $1/\text{\AA}$ ) and  $0.1$  eV bellow Fermi energy. Based on the hexagonal cell, in total, there are five different compositions by atom substitutions for the alloy, and two of them can host WSM phase. Therefore, it has a large possibility to archive Weyl points close to Fermi level in Bi-Sb alloy, and our DFT calculations is in good agreement with the unusual transport properties observed in experiments<sup>34,35</sup>.

## IV. CONCLUSION

In conclusion, we investigated the influence of atomic composition and arrangement on the topology of  $\text{Bi}_{1-x}\text{Sb}_x$  alloy via *ab-initio* calculations. Increasing the concentration of Sb, topological phase transition happens in  $\text{Bi}_{1-x}\text{Sb}_x$ . Interestingly, the atomic arrangements for a particular compositions in  $\text{Bi}_{1-x}\text{Sb}_x$  remarkably relates to its own topological feature in contrast to the previous researches that just emphasizes the effect of composition. As a result, two WSM states were obtained at  $x = 0.5$  and  $x = 0.87$  with specific atomic arrangement with the absence of inversion symmetry.

Our result is helpful for the understanding of recently unusual transport properties observed in experiments. This work reveals the importance of the combination of elemental composition and their specific arrangement for the comprehensive understanding of topological phases in Bi-Sb alloys.

## ACKNOWLEDGMENTS

This work was financially supported by the European Research Council (ERC) Advanced Grant (No. 291472) 'IDEA Heusler' and ERC Advanced Grant (No. 742068) 'TOPMAT'.

- 
- \* ysun@cpfs.mpg.de
- <sup>1</sup> X. G. Wan, A. M. Turner, A. Vishwanath, and S. Y. Savrasov, *Phys. Rev. B* **83**, 205101 (2011).
  - <sup>2</sup> G. E. Volovik, *The Universe in A Helium Droplet* (Clarendon Press, Oxford, 2003).
  - <sup>3</sup> S.-Y. Xu, I. Belopolski, N. Alidoust, M. Neupane, G. Bian, C. Zhang, R. Sankar, G. Chang, Y. Zhujun, C.-C. Lee, H. Shin-Ming, H. Zheng, J. Ma, D. S. Sanchez, B. Wang, A. Bansil, F. Chou, P. P. Shibayev, H. Lin, S. Jia, and M. Z. Hasan, *Science* **349**, 613 (2015).
  - <sup>4</sup> B. Q. Lv, H. M. Weng, B. B. Fu, X. P. Wang, H. Miao, J. Ma, P. Richard, X. C. Huang, L. X. Zhao, G. F. Chen, Z. Fang, X. Dai, T. Qian, and H. Ding, *Phys. Rev. X* **5**, 031013 (2015).
  - <sup>5</sup> L. X. Yang, Z. K. Liu, Y. Sun, H. Peng, H. F. Yang, T. Zhang, B. Zhou, Y. Zhang, Y. F. Guo, M. Rahn, D. Prabhakaran, Z. Hussain, S. K. Mo, C. Felser, B. Yan, and Y. L. Chen, *Nat. Phys.* **11**, 728 (2015).
  - <sup>6</sup> Z. K. Liu, L. X. Yang, Y. Sun, T. Zhang, H. Peng, H. F. Yang, C. Chen, Y. Zhang, Y. F. Guo, D. Prabhakaran, M. Schmidt, Z. Hussain, S.-K. Mo, C. Felser, B. Yan, and Y. L. Chen, *Nat. Mater.* **15**, 27 (2016).
  - <sup>7</sup> S.-Y. Xu, N. Alidoust, I. Belopolski, Z. Yuan, G. Bian, T.-R. Chang, H. Zheng, V. N. Strocov, D. S. Sanchez, G. Chang, C. Zhang, D. Mou, Y. Wu, L. Huang, C.-C. Lee, S.-M. Huang, B. Wang, A. Bansil, H.-T. Jeng, T. Neupert, A. Kaminski, H. Lin, S. J. Jia, and M. Z. Hasan, *Nat. Phys.* **11**, 748 (2015).
  - <sup>8</sup> I. Belopolski, S.-Y. Xu, D. S. Sanchez, G. Chang, C. Guo, M. Neupane, H. Zheng, C.-C. Lee, S.-M. Huang, G. Bian, N. Alidoust, T.-R. Chang, B. Wang, X. Zhang, A. Bansil, H.-T. Jeng, H. Lin, S. Jia, and M. Z. Hasan, *Phys. Rev. Lett.* **116**, 066802 (2016).
  - <sup>9</sup> N. Xu, H. M. Weng, B. Q. Lv, C. E. Matt, J. Park, F. Bisti, V. N. Strocov, D. Gawryluk, E. Pomjakushina, K. Conder, N. C. Plumb, M. Radovic, G. Autès, O. V. Yazyev, Z. Fang, X. Dai, T. Qian, J. Mesot, H. Ding, and M. Shi, *Nat. Commun.* **7**, 11006 (2016).
  - <sup>10</sup> S. Souma, Z. Wang, H. Kotaka, T. Sato, K. Nakayama, Y. Tanaka, H. Kimizuka, T. Takahashi, K. Yamauchi, T. Oguchi, K. Segawa, and Y. Ando, *Phys. Rev. B* **93**, 161112 (2016).
  - <sup>11</sup> H. Inoue, A. Gyeenis, Z. Wang, J. Li, S. W. Oh, S. Jiang, N. Ni, B. A. Bernevig, and A. Yazdani, *Science* **351**, 1184 (2016).
  - <sup>12</sup> R. Batabyal, N. Morali, N. Avraham, Y. Sun, M. Schmidt, C. Felser, A. Stern, B. Yan, and H. Beidenkopf, *Sci. Adv.* **2**, e1600709 (2016).
  - <sup>13</sup> H. Zheng, S.-Y. Xu, G. Bian, C. Guo, G. Chang, D. S. Sanchez, I. Belopolski, C.-C. Lee, S.-M. Huang, X. Zhang, R. Sankar, N. Alidoust, T.-R. Chang, F. Wu, T. Neupert, F. Chou, H.-T. Jeng, N. Yao, A. Bansil, S. Jia, H. Lin, and M. Z. Hasan, *ACS Nano* **10**, 1378 (2016).
  - <sup>14</sup> X. Huang, L. Zhao, Y. Long, P. Wang, D. Chen, Z. Yang, H. Liang, M. Xue, H. Weng, Z. Fang, X. Dai, and G. Chen, *Phys. Rev. X* **5**, 031023 (2015).
  - <sup>15</sup> C.-L. Zhang, S.-Y. Xu, I. Belopolski, Z. Yuan, Z. Lin, B. Tong, G. Bian, N. Alidoust, C.-C. Lee, S.-M. Huang, T.-R. Chang, G. Chang, C.-H. Hsu, H.-T. Jeng, M. Neupane, D. S. Sanchez, H. Zheng, J. Wang, H. Lin, C. Zhang, H.-Z. Lu, S.-Q. Shen, T. Neupert, M. Zahid Hasan, and S. Jia, *Nat. Commun.* **7**, 10735 (2016).
  - <sup>16</sup> Z. Wang, Y. Zheng, Z. Shen, Y. Zhou, X. Yang, Y. Li, C. Feng, and Z.-A. Xu, *arXiv:1506.00924* (2015), 1506.00924.
  - <sup>17</sup> A. C. Niemann, J. Gooth, S.-C. Wu, S. Bäßler, P. Sergeius, R. Hühne, B. Rellinghaus, C. Shekhar, V. Suß, M. Schmidt, C. Felser, B. Yan, and K. Nielsch, *Sci. Rep.* **7**, srep43394 (2017).
  - <sup>18</sup> C. Shekhar, A. K. Nayak, Y. Sun, M. Schmidt, M. Nicklas, I. Leermakers, U. Zeitler, Y. Skourski, J. Wosnitza, Z. Liu, Y. Chen, W. Schnelle, H. Borrmann, Y. Grin, C. Felser, and B. Yan, *Nat. Phys.* **11**, 645 (2015).
  - <sup>19</sup> N. J. Ghimire, Y. Luo, M. Neupane, D. J. Williams, E. D. Bauer, and F. Ronning, *J. Phys. Condens. Matter* **27**, 152201 (2015).
  - <sup>20</sup> Y. Luo, N. J. Ghimire, M. Wartenbe, H. Choi, M. Neupane, R. D. McDonald, E. D. Bauer, J. Zhu, J. D. Thompson, and F. Ronning, *Phys. Rev. B* **92**, 205134 (2015).
  - <sup>21</sup> P. J. W. Moll, A. C. Potter, N. L. Nair, B. J. Ramshaw, K. A. Modic, S. Riggs, B. Zeng, N. J. Ghimire, E. D. Bauer, R. Kealhofer, F. Ronning, and J. G. Analytis, *Nat. Commun.* **7**, 12492 (2016).
  - <sup>22</sup> A. A. Burkov and L. Balents, *Phys. Rev. Lett.* **107**, 127205 (2011).
  - <sup>23</sup> G. Xu, H. Weng, Z. Wang, X. Dai, and Z. Fang, *Phys. Rev. Lett.* **107**, 186806 (2011).

- <sup>24</sup> Y. Sun, Y. Zhang, C. Felser, and B. Yan, *Phys. Rev. Lett.* **117**, 146403 (2016).
- <sup>25</sup> E. Liu, Y. Sun, L. Muechler, A. Sun, L. Jiao, J. Kroder, V. S. H. Borrmann, W. Wang, W. Schnelle, S. Wirth, S. T. B. Goennenwein, and C. Felser, *arXiv:1712.06722* (2017).
- <sup>26</sup> W. Shi, L. Muechler, K. Manna, K. K. Zhang, Yang, R. Car, J. v. d. Brink, C. Felser, and Y. S. Sun, *arXiv:1801.03273* (2018).
- <sup>27</sup> J. Gooth, A. C. Niemann, T. Meng, A. G. Grushin, K. Landsteiner, B. Gotsmann, F. Menges, M. Schmidt, C. Shekhar, V. Sueß, R. Huehne, B. Rellinghaus, C. Felser, B. Yan, and K. Nielsch, *arXiv* (2017), 1703.10682v1.
- <sup>28</sup> C. R. Rajamathi, U. Gupta, N. Kumar, H. Yang, Y. Sun, V. Suß, C. Shekhar, M. Schmidt, H. Blumtritt, P. Werner, B. Yan, S. Parkin, C. Felser, and C. N. R. Rao, *Adv. Mater.* **54**, 1606202 (2017).
- <sup>29</sup> L. Fu and C. L. Kane, *Phys. Rev. B* **76**, 045302 (2007).
- <sup>30</sup> D. Hsieh, D. Qian, L. Wray, Y. Xia, Y. S. Hor, R. J. Cava, and M. Z. Hasan, *Science* **302**, 92 (2003).
- <sup>31</sup> M. Z. Hasan and C. L. Kane, *Rev. Mod. Phys.* **82**, 3045 (2010).
- <sup>32</sup> J. C. Y. Teo, L. Fu, and C. L. Kane, *Phys. Rev. B* **78**, 045426 (2008).
- <sup>33</sup> H.-J. Zhang, C.-X. Liu, X.-L. Qi, X.-Y. Deng, X. Dai, S.-C. Zhang, and Z. Fang, *Phys. Rev. B* **80**, 085307 (2009).
- <sup>34</sup> D. Shin, Y. Lee, M. Sasaki, Y. H. Jeong, F. Weickert, J. B. Betts, H.-J. Kim, K.-S. Kim, and J. Kim, *Nature Materials* **16**, 1096 (2017).
- <sup>35</sup> H.-J. Kim, K.-S. Kim, J.-F. Wang, M. Sasaki, N. Satoh, A. Ohnishi, M. Kitaura, M. Yang, and L. Li, *Phys. Rev. Lett.* **111**, 246603 (2013).
- <sup>36</sup> G. Kresse and J. Furthmüller, *Phys. Rev. B* **54**, 11169 (1996).
- <sup>37</sup> J. P. Perdew, K. Burke, and M. Ernzerhof, *Phys. Rev. Lett.* **77**, 3865 (1996).
- <sup>38</sup> A. A. Mostofi, J. R. Yates, Y.-S. Lee, I. Souza, D. Vanderbilt, and N. Marzari, *Comput. Phys. Commun.* **178**, 685 (2008).
- <sup>39</sup> M. P. L. Sancho, J. M. L. Sancho, and J. Rubio, *Phys. F: Met. Phys* **14** (1984).
- <sup>40</sup> M. P. L. Sancho, J. M. L. Sancho, and J. Rubio, *Phys. F: Met. Phys* **15** (1985).